Available online at www.sciencedirect.com

ScienceDirect

Procedia Manufacturing 34 (2019) 440–445

Procedia MANUFACTURING

www.elsevier.com/locate/procedia

47th SME North American Manufacturing Research Conference, Penn State Behrend Erie, Pennsylvania, 2019

Axial strategy for ultraprecise single point cutting of V-grooves Case 1: constant chip thickness

Delfim Joao[a,b], Nicolas Milliken[b,a], Evgueni V. Bordatchev[b,a]*, O. Remus Tutunea-Fatan[a,b]*

[a]*Western University, London, Canada*
[b]*National Research Council of Canada, London, Canada*

* Corresponding authors: Tel.: +1-226-688-5604; fax: +1-519-430-7064. *E-mail address:* Evgueni.Bordatchev@nrc-cnrc.gc.ca
Tel.: +1-519-661-2111 x88289; fax: +1-519-661-3020. *E-mail address:* rtutunea@eng.uwo.ca

Abstract

V-groove microstructures have found numerous applications in mechanical, electronic, photonic, bio-mechanical and optical components. However, despite their relatively wide use, the manufacturing strategies associated with the fabrication of V-grooves were little investigated so far. To address this, the current study provides an analytical formulation of the conventional axial strategy for ultraprecise single point cutting of V-grooves characterized by a constant chip thickness. Furthermore, multi-pass path planning and its practical implementation are described with respect to the variable cross-sectional area. Experimentally measured cutting forces and resulted surface quality are also reported in this study. The results obtained validate a predictable linear dependence between chip thickness, area being cut, cutting force amplitude and areal average surface roughness.

Keywords: V-groove fabrication; ultraprecise single point cutting; constant chip thickness

1. Introduction

V-grooves represent one of the important microstructures that have found numerous applications in mechanical, electronic, photonic, biomechanical and optical components [1]. Their wide use can be attributed to their capability to enhance surfaces with numerous types of additional functionalities [2]. In recent years, much of the V-groove use was devoted to optical component such as retroflectors [3], light guides [4], fiber positioning systems [5, 6], and solar energy harvesting [7, 8]. In almost all these instances the core V-groove functionality included beam splitting and/or light concentration/focusing [9-11].

The techniques used in V-groove fabrication can be roughly subdivided into two main groups, essentially involving rotational or non-rotational cutting tools [12, 13]. Past studies involving rotational tools noted that although this machining approach is very good for shape accuracy and surface quality, long slopes tend to be produced at the flat ends of the microgrooves [14]. By contrast, grooves generated with non-rotational tools revealed that the characteristic slopes that are present at the end of microstructure are shorter. Furthermore, this cutting technique tends to be more versatile in a sense that it enables the generation of microgrooves with a broad variety of curvatures [14]. The aforementioned slope reductions are primarily influenced by the tighter control of the tool/workpiece angle entrance and exit [14]. Both manufacturing variants can produce V-groove microstructures with submicron dimensional accuracies and nanometric surface roughness [15]. However, the surveyed literature shows that not much progress has been reported so far on the development of specific V-groove cutting strategies.

To date, V-grooves were produced through several different fabrication methods such as: flycutting [16], raster

10.1016/j.promfg.2019.06.189

milling [17], and precision grinding [15]. The latter method proved to be an effective technique for non-ferrous and difficult-to-machine materials, particularly due to its reduced tool wear [18]. Nevertheless, precision grinding remains a time consuming and hence expensive process. By contrast, fly-grooving experiments performed on monocrystalline silicon verified that fly-cutting is appropriate for the ductile removal of brittle materials since it generates large compressive pressures in the chip formation zone [19]. Finally, ultraprecision raster milling was noted to produce non-symmetric freeform surface with nanometric surface finish and submicron form accuracy without the need for additional postprocessing [17].

2. Ultraprecise single point cutting

Ultraprecise single point cutting is one of the most common types of non-rotational cutting processes used to generate V-grooves. In this context, the use of the single point diamond tool enables cost-effective generation of nanometer-range roughness [20].

Figure 1 illustrates the geometry of the tool used in this study, essentially consisting of a monocrystalline diamond insert and its holder. In terms of diamond insert design, the rake angle was set at 0°, whereas the clearance angle was prescribed at 10°. However, the most important tool design characteristic remains the included angle of 90° that enables the generation of a symmetric V-groove profile.

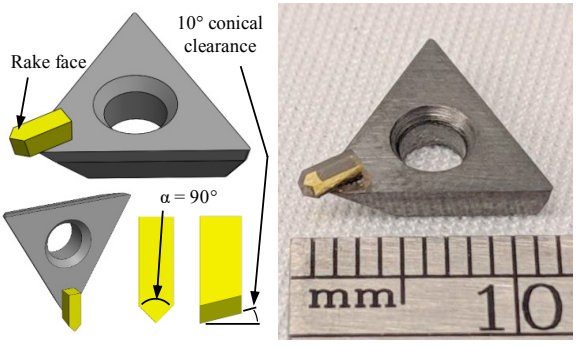

Fig. 1. V-shaped monocrystalline diamond single point cutting tool.

3. Machine setup and process kinematics

A schematic, but detailed representation of the experimental setup is depicted in Figure 2. In brief, the core element of the machine setup is represented by the Kugler Microgantry Nano 5x micromachining center. To capture the three principal axis components of the cutting force, a three-axis Kistler 9256C2 dynamometer was mounted atop of the machine tool C-axis and underneath of the workpiece.

The signal captured by the dynamometer was amplified in a Kistler Dual Mode Amplifier and it was also split into *X*, *Y*, and *Z* components. The amplifier was connected to a National Instruments terminal block BNC 2110 to allow signal monitoring on a LeCroy Wayerunner LT354 oscilloscope. From the terminal block, the signals were also transferred to a National Instruments 6023e data acquisition card to enable their storage for subsequent processing.

The cutting strategy to be presented further was termed as "axial" due to the inherent nature of its kinematics. More specifically – as shown in Figure 3a – the tip of diamond tool remains aligned with the workpiece coordinate system that is always located at the center of the V-groove profile. The cutting motion remains contained in the YZ plane (see Figure 3b) such that P_aP_b represents the length during which the tool remains in contact with the workpiece.

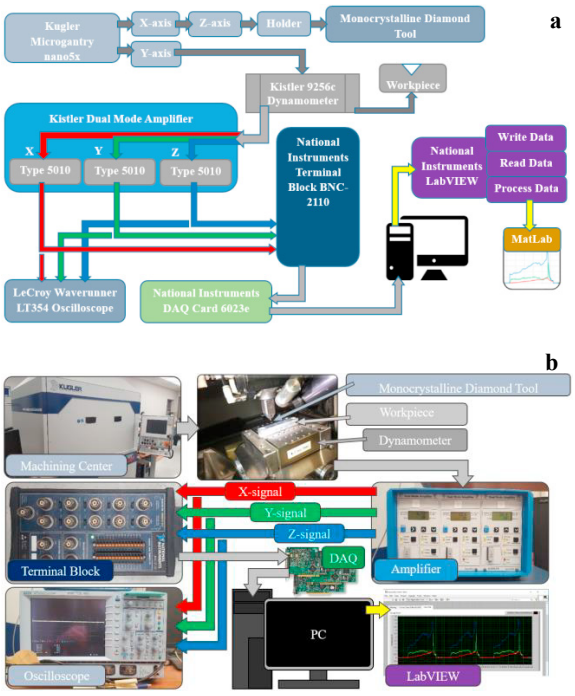

Fig. 2. Experimental setup representations:
(a) block diagram; (b) photographic.

The tool follows a pattern consisting of a sequence of down-across-up-return-down-repeat motions. According to this sequence, the tool moves up (at P_b) to the same Z height during the ancillary return motion and moves down at P_a in preparation of a new cut. The "down" motion at the beginning of a new "across" path is always positioned at the bottom of the groove that will be cut (Figure 3c). Clearly, the distance between the P_1, P_2, P_3, points is constant and is determined by the preset chip thickness (δ_{th}). The only exception from this rule might be constituted by the last cut across pass that might happen at layer thickness smaller than δ_{th}.

4. Axial cutting strategy with constant chip thickness

As indicated in the previous section, the current strategy was

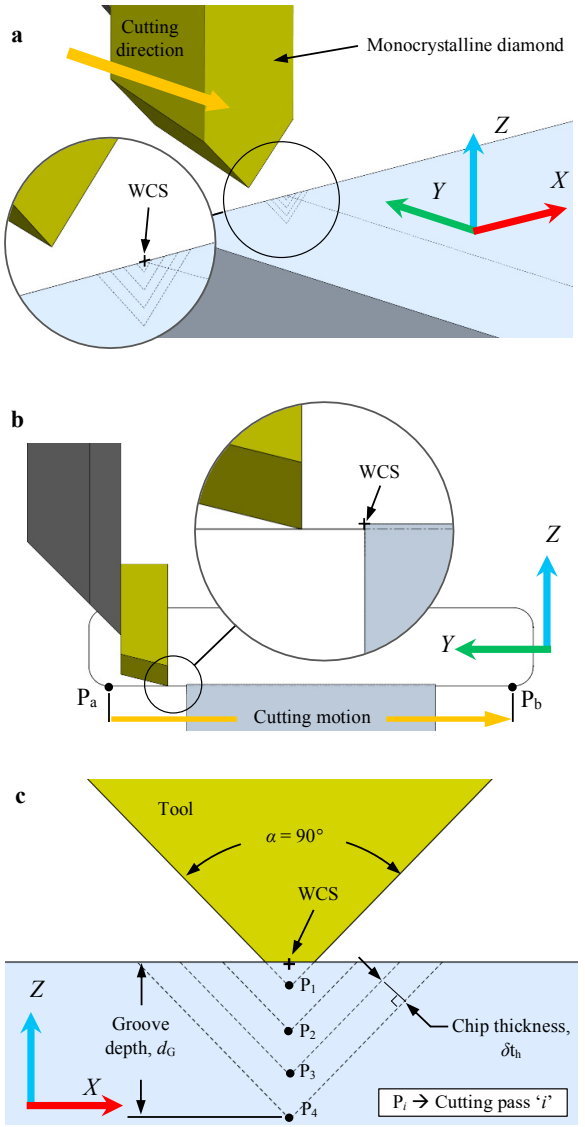

Fig. 3. Cutting kinematics: (a) isometric view; (b) side view along +*X* direction; (c) front view along +*Y* direction.

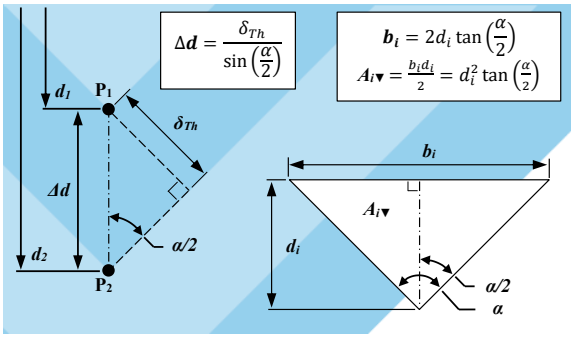

Fig. 4. Geometric parameters associated with the symmetrical V-groove characterized by an included angle α.

termed axial, primarily because tool motion happens only in one plane that becomes incrementally deeper into the V-groove structure. According to this approach/cutting strategy, it will be hypothesized here that the cut area will increase linearly proportional with the number of passes across the workpiece. Of note, "number of passes" are equivalent with depth of cut within a certain V-groove.

The small chip thickness (< 20 µm) and workpiece surface tolerances make the accurately setting of the *Z*-height relatively difficult. Because of this, the first cut at d_1 is always accompanied by an inherent error. By assuming that this error is within the range of Δd $(\Delta d = d_n - d_{n-1})$, then: $d_1 = \Delta d^{+0.0}_{-\Delta d}$. In this strategy, Δd is assumed as constant, therefore after the first cutting pass, the depth can be calculated as $d_n = (d_{n-1} + \Delta d)^{+0.0}_{-\Delta d}$. Based on the error in d_1 and by assuming that a negligible manufacturing error is associated with tool's included angle (α), the error with respect to the cross-section area can be determined as $e_A = A^{+0.0}_{-\Delta d^2}$.

$$\Delta d = \frac{\delta_{\text{th}}}{\sin\left(\frac{\alpha}{2}\right)} \tag{1}$$

$$b_i = 2d_i \tan\left(\frac{\alpha}{2}\right) \tag{2}$$

$$A_{\Delta} = \frac{b_i d_i}{2} = d_i^{\,2} \tan\left(\frac{\alpha}{2}\right) \tag{3}$$

$$A_i = A_{\Delta} - A_{(i-1)\Delta} \tag{4}$$

In the above relationships, Equation 3 yields the cutting area of the first cut (i.e., a complete triangle in Figure 4). However, this calculation is no longer valid for the subsequent cuts whose areas are outlined by the alternating blue-toned colors in Figure 5a that require instead triangular area subtractions.

The results of the cut area calculations were represented in a graphical form in Figure 5b. Here, the linear trend is obvious and expected and it will be verified further against the experimental measurements of the main component of the cutting force obtained in a perpendicular-to-feed or *Y*-axis direction.

5. Experimental results

The axial cutting strategy was tested on an aluminum block (Figure 2b). Table 1 summarizes the experimental parameters used in the current study.

Table 1. Summary of experimental conditions

Feed rate (mm/min)	500
Chip thickness (µm)	5, 10, 15
Coolant	Isoparaffin mist

Following data acquisition procedure, advanced signal analysis was applied to the recorded data using Matlab software. Initially, LabView-formated data was converted to text only format for further storage and processing. After that, high-frequency noise was filtered out by means of a low-pass filter with a 10 Hz cutoff frequency.

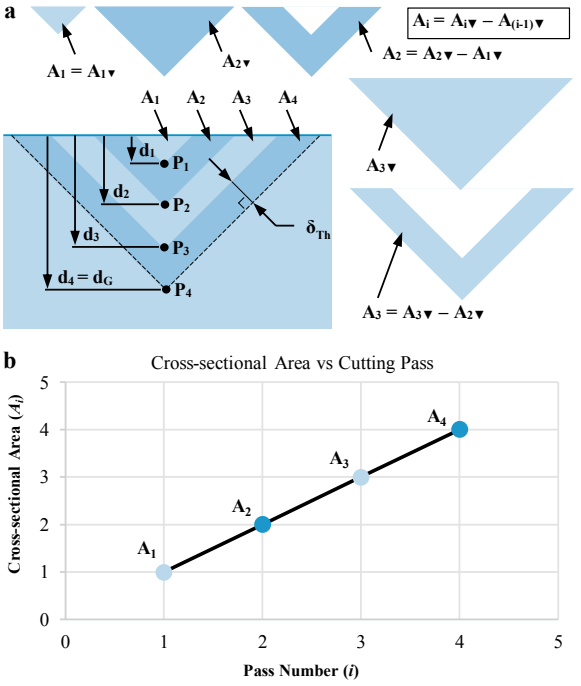

Fig. 5. Dependence between cutting area and cutting pass: (a) geometric characteristics; (b) graphical representation.

This particular sequence of data postprocessing enabled a correct determination of the quasi-static component of the cutting process only that is directly related to the chip thickness and corresponded cut area. Figure 6a shows raw-filtered data for a chip chickness of 10 µm. Each pulse of the cutting force signal is associated with a new pass across the flat surface of the workpiece. While the dynamometer has captured some weak signals for X and Z components of the cutting force, the analysis presented herein will remain focused on F_Y only since this represents the main component along the feed direction.

While processing the cutting force data, a certain drift of the measurement system drift became noticeable for all three components of the cutting force. To eliminate the drift, first order linear regression data was used to determine the mean of the data to be brought down to zero, essentially corresponding to noncontact situations between tool and workpiece. Once the slope of the drifting mean was determined, appropriate values were subtracted across the entire cutting force domain, such that the drift was eventually eliminated for all three components of the cutting force (Figure 6b).

A more careful analysis of the data presented in Figure 6c reveals that F_Y signal fluctuations are present. While their actual root cause remains unclear at this time, it can be

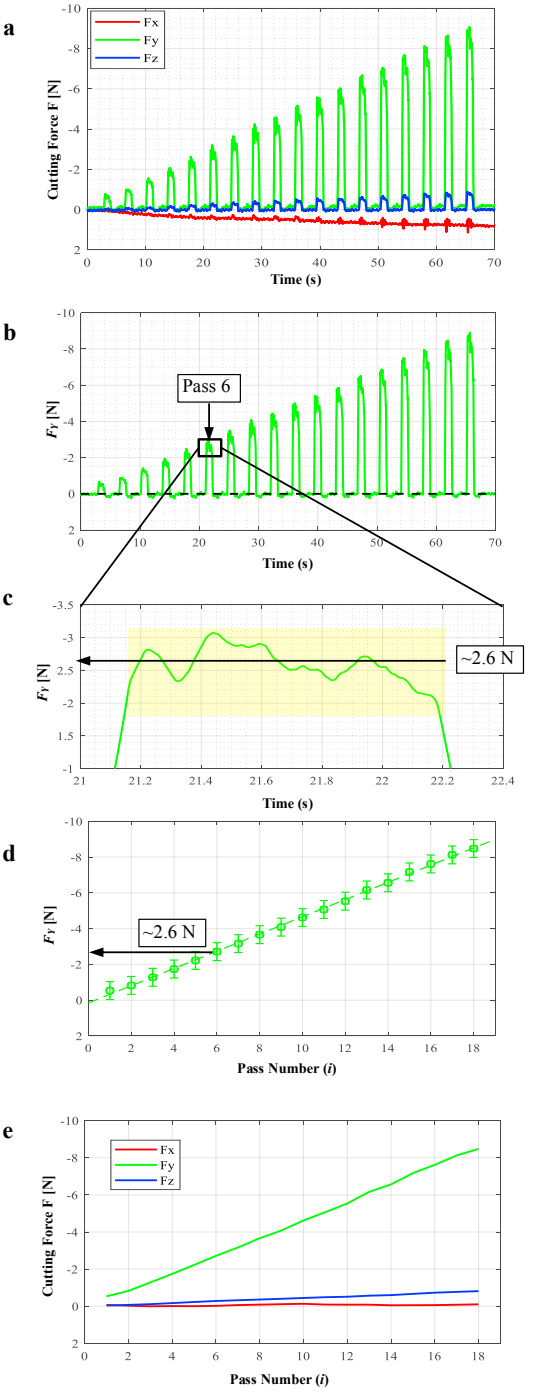

Fig. 6. Cutting force measurements: (a) raw data; (b) F_Y with measurement drift corrected; (c) sample of average F_Y calculation; (d) average F_Y variation during microgroove cutting; (e) average cutting force components.

assumed that they have could be a consequence of the initial impact between tool and workpiece as well as inconsistent chip removal phenomena. To process these variable pulses,

the peak F_Y values were averaged for each V-groove cut/pulse across the workpiece and then plotted against passes (Figure 6d). The error bars represent the standard deviation of the raw but drift-corrected acquired data (Figure 6b).

Figure 6e illustrates graphical representation of all cutting force components for the entire duration of V-groove cutting.

According the these results, while F_X nears zero – and this remains consistent with the overall tool kinematics – F_Z has nonzero values, most likely due to the upward force exerted by the chip on the tool. According to the prior predictions, F_Y component follows a linear dependence with respect to the number of passes. Moreover, a strict dependence to chip thickness also exists (see Fig. 7).

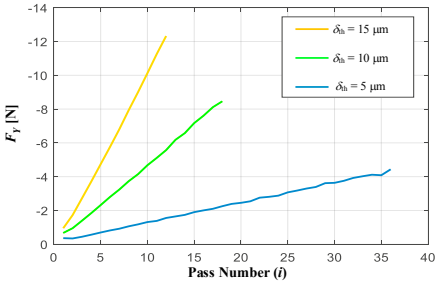

Fig. 7. Correlation between the main component of the cutting force and chip thickness.

In addition to cutting force results, quality of V-groove surface was assessed by means of an optical profilometer. For this purpose, workpiece was tilted at an angle of 45°. This was required to enable a horizontal positioning of the V-groove facets, an essential prerequisite of an accurate surface quality measurement. A representative illustration of V-groove surface topography is presented in Figure 8. The spatial inclination/tilt that is present and visible in the raw data (Figure 8a) was corrected in such a way that its mean was positioned on zero (Figure 8b). Then, a filter with a cutoff wavelength of 80 µm (ISO 16610-61) was applied to remove surface waviness and retain just its roughness. The final postprocessed topographic data is presented Figures 8c-e for various chip thickness values whereas Table 2 summarizes the results of the areal average surface roughness measurements (S_a). These results imply that optical surface quality (< 10 nm) is attainable by means of the proposed single point cutting procedure.

Table 2. Summary of surface quality measurements

Chip thickness (µm)	S_a (nm)
5	5.4128
10	5.7310
15	14.895

6. Summary and Conclusions

The current study presents a cutting strategy to be used during V-groove fabrication through ultraprecise single point cutting. According to the outlined axial cutting approach, the profile of the groove is produced by maintaining a constant thickness of the cut. The comparison performed between analytical and experimental results revealed that a linear relationship exists between the number of passes/depth of the cut and the magnitude of the cutting force as measured along the feed direction. This is a clear a consequence of the direct proportionality between the quasi-static components of the cutting force and the area and volume of material being removed at each pass.

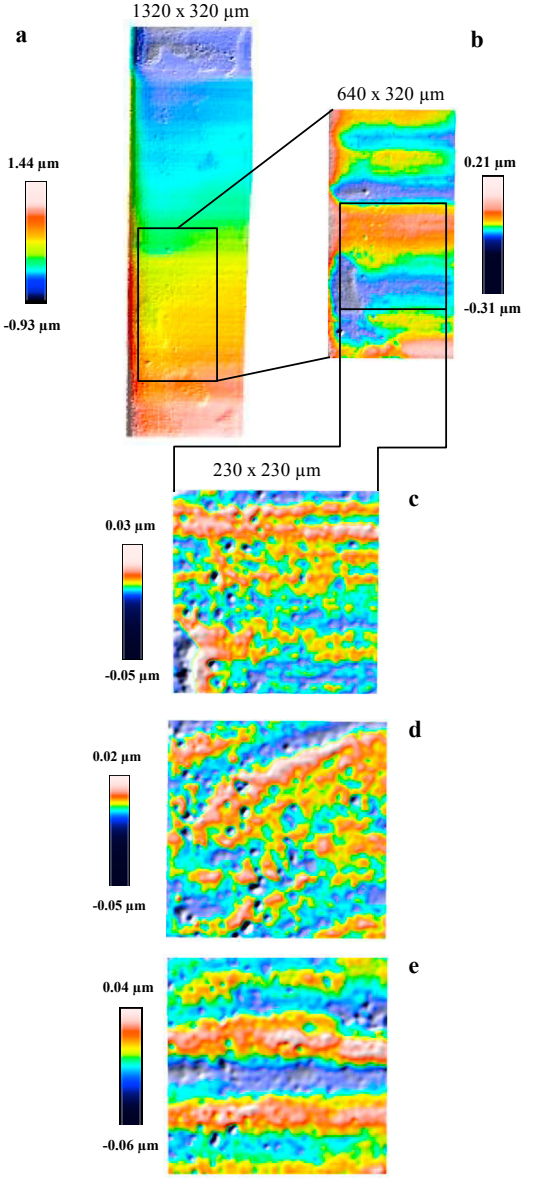

Fig.8. Surface quality results: (a) raw data; (b) data with planar tilt removed; V-groove surface topography for: c) 5 µm chip thickness; 10 µm chip thickness; (e) 15 µm chip thickness.

In addition, the results of the surface topography measurements have confirmed that the investigated strategy is not only capable of producing ultraprecise surfaces, but it was also demonstrated that smaller chip thicknesses produce a better surface quality as typically expected and implemented in machining practice.The most significant contributions of the present study revolve around the analytical formulation presented multi-pass single point cutting of V-grooves with constant chip thickness. The experimental data acquired on cutting force magnitude has validated the analytically inferred linear dependence between the area of the material being removed and depth of cut/number of passes. However, other effects – that were potentially attributed to chip removal challenges and/or initial shock/contact between tool and workpiece – were also present in a sense that cutting forces did not have a perfectly constant magnitude during V-groove cutting.

The analysis presented in the current study sets the foundation for further development of future and more efficient cutting strategies to be used in ultraprecise single point cutting of V-grooves. Among them, constant cutting area and non-axial cutting strategies will represent an immediate investigational priority. Furthermore, simulation models of the cutting mechanics will be developed and then validated against the acquired experimental results.

Acknowledgements

The work presented in this study is the result of the collaboration between Western University (London, Ontario) and National Research Council of Canada (London, Ontario). Partial financial support was also provided by Natural Sciences and Engineering Research Council (NSERC) of Canada.

References

[1] Fang F, Wu H, Liu X, Lim G, Liu Y, Ng S. Fabrication of micro grooves. Proceedings of ASPE 18th Annual Meeting, Portland, USA. 2003.
[2] Brinksmeier E, Gläbe R, Schönemann L. Diamond Micro Chiseling of large-scale retroreflective arrays. Precision Engineering-Journal of the International Societies for Precision Engineering and Nanotechnology. 2012;36:650-7.
[3] Lin C-Y, Su C-H, Hsu c-m, Lin C-R. Improvement of the Microcrystalline Cube Corner Reflective Structure and Efficiency. 2008.
[4] Li P, Xie J, Cheng J, Wu KK. Anisotropic wetting properties on a precision-ground micro-V-grooved Si surface related to their micro-characterized variables. Journal of Micromechanics and Microengineering. 2014;24:075004.
[5] Zhong ZW, Lim SC, Asundi A. Effects of thermally induced optical fiber shifts in V-groove arrays for optical MEMS. Microelectronics Journal. 2005;36:109-13.
[6] Priyadarshi A, Fen LH, Mhaisalkar SG, Kripesh V, Asundi AK. Fiber misalignment in silicon V-groove based optical modules. Optical Fiber Technology. 2006;12:170-84.
[7] Dey R, Bordatchev EV, Tauhiduzzaman M, Reshef H. Optical simulation and fabrication of periodic triangular gratings for the enhancement of photovoltaic solar panels. Proc of the SPIE. 2012;8256:82561Z.
[8] Bordatchev E, Tauhiduzzaman M, Dey R. Enhancement of photovoltaic cell performance using periodic triangular gratings. Journal of Photonics for Energy. 2014;4:044599.
[9] MacDonald C, De Cusatis C, Mahajan V, Li G, Bass M. Handbook of Optics: Volume V – Atmospheric Optics, Modulators, Fiber Optics, X-Ray and Neutron Optics, Third Edition: McGraw-Hill Companies, Inc. 2010.
[10] Fang FZ, Zhang XD, Zhang GX, Weckenmann A, Evans C. Manufacturing and measurement of freeform optics. CIRP Annals - Manufacturing Technology. 2013;62:823-46.
[11] Sezerman O, Aghdam NY, Nguyen T, Rock HW. Stress relief in fibre optic arrays. United States: Oz Optics Limited, Carp (CA) 2005.
[12] Suzuki H, Moriwaki T, Yamamoto Y, Goto Y. Precision cutting of aspherical ceramic molds with micro PCD milling tool. CIRP Annals-Manufacturing Technology. 2007;56:131-4.
[13] Flucke C, Gläbe R, Brinksmeier E. Diamond micro chiselling: cutting of prismatic micro optic arrays. Proc 7th Int Conf European Society for Precision Engineering and Nanotechnology $($ EUSPEN $) $, Bremen, Germany, 20–24 May 2007. 2007.
[14] Moriya T, Nakamoto K, Ishida T, Takeuchi Y. Creation of V-shaped microgrooves with flat-ends by 6-axis control ultraprecision machining. CIRP annals. 2010;59:61-6.
[15] Wang SJ, Chen X, Liu Q, Zhou CQ, Liu JQ, Yin ZQ. Development of a precision grinding machine system for the fabrication of micro V-grooves array. The International Journal of Advanced Manufacturing Technology. 2018;97:2141-50.
[16] Fang F, Liu Y. On minimum exit-burr in micro cutting. Journal of Micromechanics and Microengineering. 2004;14:984.
[17] Wang S, To S, Chen X, Wang H, Xia H. A study of the fabrication of v-groove structure in ultra-precision milling. International Journal of Computer Integrated Manufacturing. 2014;27:986-96.
[18] Butler-Smith P, Axinte D, Daine M. Ordered diamond micro-arrays for ultra-precision grinding—an evaluation in Ti–6Al–4V. International Journal of Machine Tools and Manufacture. 2011;51:54-66.
[19] Peng Y, Jiang T, Ehmann K. Research on single-point diamond fly-grooving of brittle materials. The International Journal of Advanced Manufacturing Technology. 2014;75:1577-86.
[20] Rezaur Rahman K, Rahman M, Neo K, al. e. Micro-grooving on electroless nickel plated die materials. The International Journal of Advanced Manufacturing Technology. 2006;27:911-7.